JOURNAL OF THEORETICAL AND APPLIED MECHANICS
49, 2, pp. 477-499, Warsaw 2011

INVESTIGATIONS OF AERODYNAMICS OF TESLA BLADELESS MICROTURBINES

Piotr Lampart
Łukasz Jędrzejewski

The Szewalski Institute of Fluid Flow Machinery, Polish Academy of Sciences, Gdańsk, Poland
lampart@imp.gda.pl; jedrzejewski@imp.gda.pl

The paper presents an analysis of a Tesla bladeless turbine for a co-generating micro-power plant of heat capacity 20 kW, which operates in an organic Rankine cycle with a low-boiling medium. Numerical calculations of the flow in several Tesla turbine models are performed for a range of design parameters. Results of the investigations exhibit interesting features in the distribution of flow parameters within the turbine interdisk space. The efficiency of the Tesla turbine depends on many parameters, including pressure, temperature and velocity conditions, rotational speed of the rotor as well as on the number, diameter, distance between the disks and the state of the disk surface and, finally, on the number and arrangement of the supply nozzles. The calculated flow efficiences of the investigated Tesla turbine models show that the best obtained solutions can be competitive as compared with classical small bladed turbines.

Key words: bladeless frictin turbine, flow efficiency, CFD simulation

1. Introduction

The first bladeless turbine, also known as a friction turbine, was designed and manufactured by a Serbian engineer and inventor Nicola Tesla in 1913 (Tesla, 1913). This unusual device makes use of viscous effects which occur in the boundary layer flow. Opposite to classical bladed turbines, where viscous effects in flow are undesirable as a source of efficiency loss, these effects enable rotational movement of the rotor. The rotor consists of up to a few dozens of thin disks locked on a shaft perpendicular to its axis of revolution. In theory, the disks should be as thin as possible. The distances, or gaps, between the disks should also be very small. According to Rice (1991), the highest value of efficiency appears when they are approximately equal to the double boundary

layer thickness. Therefore, the gaps between the disks should depend on the occurring flow conditions and physical properties of the working fluid. On the other hand, the thickness of the disks and the distances between them are also limited by the material strength and the technology of manufacture and assembly. An example of the multidisk rotor construction of the Tesla turbine found in the patent documentation (Hicks, 2005) is shown in Fig. 1.

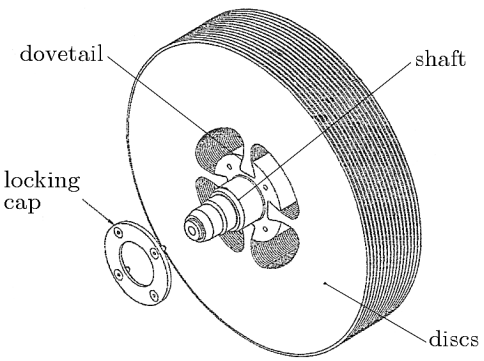

Fig. 1. Rotor of a multidisc Tesla bladeless turbine (Hicks, 2005)

The supply of the Tesla turbine is accomplished by one or several nozzles discretely located along the circumference. The nozzles are tilted under a certain angle to the disk tangent. The working fluid flows between the disks spirally from the outer to inner radius and transfers energy to the rotating disks. The medium flows out in the axial direction through a number of holes in the disks situated near the turbine shaft. The efficiency of the Tesla turbine depends on many parameters, namely on: pressure, temperature and velocity conditions between the disks, number, diameter, thickness and distance between the disks as well as on the state of the disk surface, rotational speed of the rotor, number and arrangement of the supply nozzles, etc.

In the subject-matter literature, examples of experimental research referring to the following models of Tesla micro-turbines can be found:

- ~ 1.8 kW output power, 18 000 rpm, 16% efficiency (Mikielewicz *et al.*, 2008)
- ~ 50 W output power, 1000 rpm, 21% efficiency (North, 1969)
- ~ 1.5 kW output power, 12 000 rpm, 23% efficiency (Hicks, 2005; Rice, 1965)
- ~ 1 kW output power, 12 000 rpm, 24% efficiency (Beans, 1966)
- ~ 3 kW output power, 15 000 rpm, 32% efficiency (Gruber and Earl, 1960)

- ~ 1.5 kW output power, 120 000 rpm, 49% efficiency (Davydov and Sherstyuk, 1980).

Most models listed above were tested for low rotational speeds not exceeding 18 000 rpm which makes the selection of an electric generator easy (Tesla, 1913). Experimental works aimed first of all at establishing relationships between the turbine efficiency and working parameters given below:

- distance between micro-turbine disks
- number, diameter and state of the disk surface of micro-turbine disks
- number and construction of inlet nozzles
- rotational speed of the rotor
- medium inlet pressure, temperature, velocity and angle
- corrosion and erosion of micro-turbine elements
- constructional materials (composites, ceramic materials, bronzes, aluminium alloys)
- kind of medium flowing through the micro-turbine (air, biogas, organic agents, exhaust gases, multi-phase media).

Prototypes of Tesla microturbine generators working on air or water steam were designed at Phoenix Navigation & Guidance Inc. (http://phoenixnavigation.com). They operate on up to 10.5 bar of inlet pressure and are manufactured in two options of the disk diameter:

- Turbogen-1 – 4.5" generating 250 W of electric power
- Turbogen-2 – 6.5" generating 750 W of electric power.

Examples are shown in Fig. 2. Not only turbines but also compressors, pumps and gas turbine sets can be built on the basis of the same working principle.

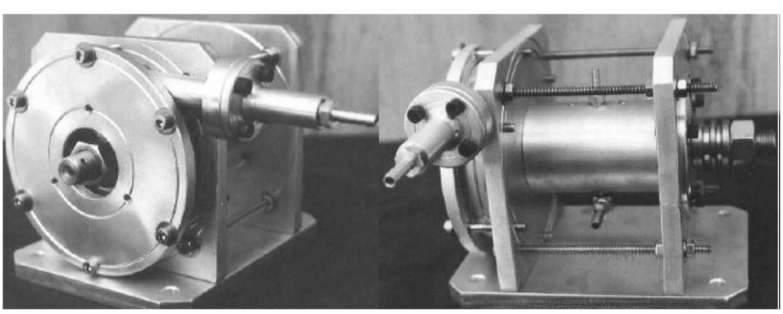

Fig. 2. 4.5" Tesla microturbines working on a water steam

There is a number of possible applications where Tesla turbines can be considered, including:

- biomass fuelled power plants
- heat recovery installations
- co-generation systems
- systems using solar energy
- plants with low temperature geothermal medium
- installations where exhaust heat can be utilized.

There are many technical benefits and a quite big potential for the construction of Tesla microturbines, especially those working in an Organic Rankine cycle, but not only (Kosowski, 2007):

- relatively high cycle and turbine efficiency (in theory)
- low mechanical stress in the turbine due to its small size and low peripheral speeds
- low speed of the turbine rotor, allowing even the direct drive of the electric generator without a reduction gear
- no erosion of blades, due to the absence of moisture (if a working fluid other than water is used)
- long lifetime
- no operator is required
- simple start-stop operation
- quiet operation
- low level of maintenance requirements
- good part load performance
- no axial loads
- easy to repair
- cheaper than bladed turbines due to the simple construction of the rotor.

Although the project of bladeless turbine is known for almost one hundred years, there are still some weak points and several issues that should be better recognized such as (Lampart *et al.*, 2009):

- the efficiency about 30% is rather too small a value
- correlations between the number of supply nozzles and the slope angle of the nozzles
- influence of the state of disk surface on the turbine efficiency

- find out the optimum degree of reaction
- negative influence of shock wave occurrence.

Most of these problems are addressed in this paper using numerical methods.

2. Computational domains

The calculation domains for the investigated models of Tesla microturbines are prepared with the help of the software Gambit (Fluent Inc., 2000). Two groups of models are analysed:

1) with the fluid outflow to the shaft,
2) with the outflow through the holes located at a certain low diameter of the disks.

The considered Tesla turbine models consist of 11 rotating disks (12 flow channels of the interdisk space). The investigations are made for two diameters of the disks – 100 mm and 300 mm. The models are equipped with two, four, six or eight supply nozzles discretely located along the circumference. Nozzle throats are carefully selected for each model to obtain the same value of the mass flow rate for a specific pressure drop referring to the nominal operating conditions. Moreover, the supply nozzles differ in slope angle – two magnitudes of inlet angle relative to the disk tangent are considered: 10° and 15°.

The first group of models represent a simplification of real geometry of Tesla turbines. The outlet area is simplified here in a way to allow the medium outflow from the turbine flow passage along the entire circumference of the shaft, in the radial direction. The presence of the tip clearance is neglected. The calculations are carried out in a fixed (motionless) reference frame, with turbine disk walls kept in rotational motion. Due to model symmetry and an assumption of flow recurrence in each interdisk passage, the computational domain contains only a half of the single interdisk space (with the flow symmetry assumed in a central interdisk plane) and supply nozzles. Figure 3 presents images of the calculation area for several turbine models (first group of models) with four, six and eight inlet nozzles. Basic geometrical parameters of particular investigated models (group 1) are given in Table 1.

The second group of models represent full geometry of 11-disk Tesla turbines with the outer casing and the radial gap above the disks. Flow symmetry is assumed which reduces the computational domain to 5 and 1/2 disks and

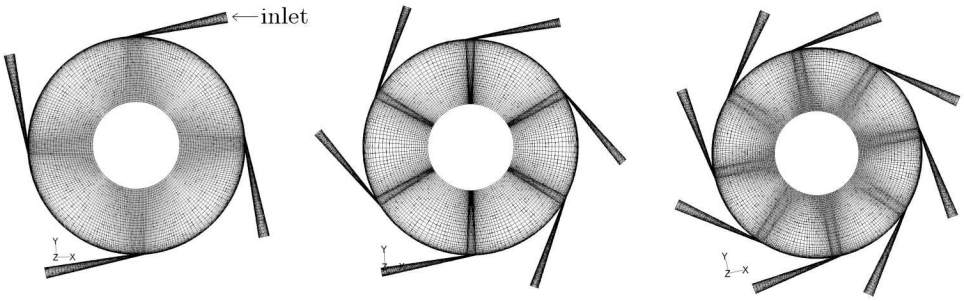

Fig. 3. Calculation domain for three different nozzle configurations of the simplified model of a Tesla turbine

Table 1. Geometrical properties of calculation domains for Tesla turbine models

No. of nozzles	Inlet angle β [deg]	Width of gap t [m]	Outer radius of the disk r_1 [m]	Inner radius of the disk r_2 [m]	No. of cells
4	10°	0.00025	0.05	0.02	398 736
4	15°	0.00025	0.05	0.02	478 656
6	10°	0.00025	0.05	0.02	396 000
6	15°	0.00025	0.05	0.02	370 800
8	10°	0.00025	0.05	0.02	540 000
8	15°	0.00025	0.05	0.02	576 000
2	10°	0.00025	0.15	0.06	1 224 000
4	10°	0.00025	0.15	0.06	1 296 000
6	10°	0.00025	0.15	0.06	1 728 000

6 flow passages. Two or four supply nozzles are considered for the investigated models. The disk diameter and thickness were assumed equal to 100 mm and 0.5 mm, respectively, whereas the interdisk space is equal to 0.25 mm. Figure 4 presents a sample image of the calculation area for several turbine models with two or four supply nozzles belonging to the second group of models.

In accordance with the assumed turbulence model, the calculation grid at the disk wall was refined so as to obtain the y^+ value equal to 1-5. The mesh was also refined in the inlet and outlet regions and in the region near the outlet from the nozzles, where the highest magnitudes of velocity occur. This is a structural mesh divided into blocks, which contains from up to 1 296 000 finite volumes (first group models) and up to 7 500 000 cells for the second group model (so far one four-nozzle model was calculated).

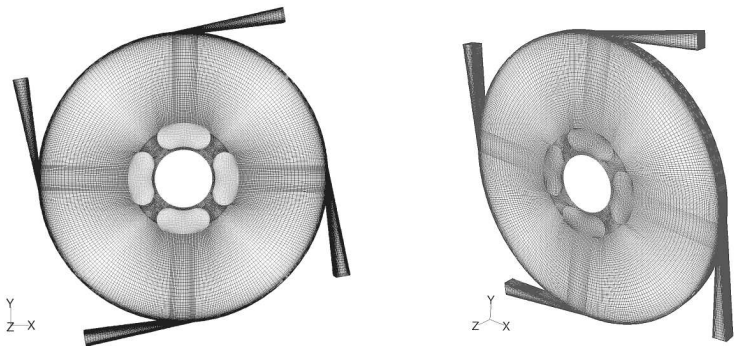

Fig. 4. Full model design of a Tesla turbine

3. Flow model

CFD calculations of various models of Tesla disk turbines were carried out on the basis of the RANS model (Wilcox, 1993) supplemented by the $k-\omega$ SST (Menter *et al.*, 2003) turbulence model available in the computer program Fluent (Fluent Inc., 2000).

Numerical discretisation of the set of fundamental equations was performed using the finite volume method. The "segregated" solver with the sequential solving of the governing equations as well as the SIMPLE algorithm for correction of pressure and velocity were applied. Discretisation of convection fluxes was performed using an "upwind" scheme of the 2nd order accuracy. The time-domain discretisation was made by an "implicit" scheme. All under-relaxation factors were lowered compared to their default values. The calculations were carried out until the stationary state was reached, lowering the residua of particular equations by 4 orders of magnitude (8 orders of magnitude for the energy residuum).

Thermodynamic parameters assumed for CFD calculations were found from preliminary 1D model calculations, making use of the data from literature sources. It is assumed that the considered Tesla turbine models consist of 11 rotating disks (12 flow channels of the interdisk space). The nominal operating conditions are for the mass flow rate of 0.13 kg/s and pressure drop from 14.8 bar to 1.9 bar. It is important that in each case the nozzles were designed to get exactly the same value of mass flow rate at the nominal point of work. Solkatherm®SES36S was assumed to be the working medium. The perfect gas model was chosen for the calculations, assuming the individual gas constant and specific heat as average values from the given expansion range. Values of dynamic viscosity and the heat conductivity coefficient were assu-

med in a similar way. Pressure boundary conditions relevant for compressible flow were assumed. However, it should be noted that the perfect gas model assumed for the calculations may be a poor approximation of working medium properties, especially for flow velocities close to the sonic velocity. The calculations were carried out for a range of operating conditions (by changing the available pressure drop from 2 bar to the nominal value) for two rotational speeds of the rotor, namely: 9 000 rpm and 18 000 rpm, giving two different work characteristics of each microturbine model.

The flow efficiency of the 11-disk turbine was calculated from the following formula

$$\xi = \frac{P}{P_{is}} = \frac{P}{GH_{is}} = \frac{M\omega}{GH_{is}} \tag{3.1}$$

where: ξ is the isentropic efficiency, P – power generated by the 11-disk turbine, P_{is} – theoretical power in isentropic conversion, M – moment of force generated on 11 disks, ω – angular speed of the disk, G – mass flow rate in the 11-disk turbine (12 interdisk gaps), H_{is} – isentropic enthalpy drop.

The isentropic drop of enthalpy can be found from the perfect gas approximation as

$$H_{is} = c_P T_{in}\Big[1 - \Big(\frac{p_{ex}}{p_{in}}\Big)^{\frac{\kappa-1}{\kappa}}\Big] \tag{3.2}$$

where: c_p is the specific heat, T_{in} – inlet temperature, p_{in} – inlet static pressure, p_{ex} – outlet static pressure, κ – ratio of specific heats.

In the case of simplified Tesla turbine models (group 1) Eq. (3.4) can be rewritten as

$$\xi = \frac{P}{P_{is}} = \frac{11P'}{12G'H_{is}} = \frac{22M'\omega}{12G'H_{is}} \tag{3.3}$$

where: P' is the power generated from a single disk, G' – mass flow rate for the single interdisk space, M' – moment of force generated on one side of the disk.

The turbine reaction is calculated here as the ratio of static pressure drop in the interdisk space related to the pressure drop in the turbine and shows which part of expansion takes place within the rotor domain

$$\rho = \frac{p_1 - p_{ex}}{p_{in} - p_{ex}} \tag{3.4}$$

where: ρ is degree of reaction, p_1 – static pressure at the nozzle outlet.

4. Analysis of numerical results

4.1. Simple model analysis

Figures 5 and 6 show contours of static pressure and velocity for sample configurations of Tesla turbine models of disk diameter 100 mm with four, six and eight supply nozzles. The images were captured at the symmetry plane of the interdisk space for two rotational velocities of the disk for nominal operating conditions (for the mass flow rate of the 11-disk turbine – 0.13 kg/s and

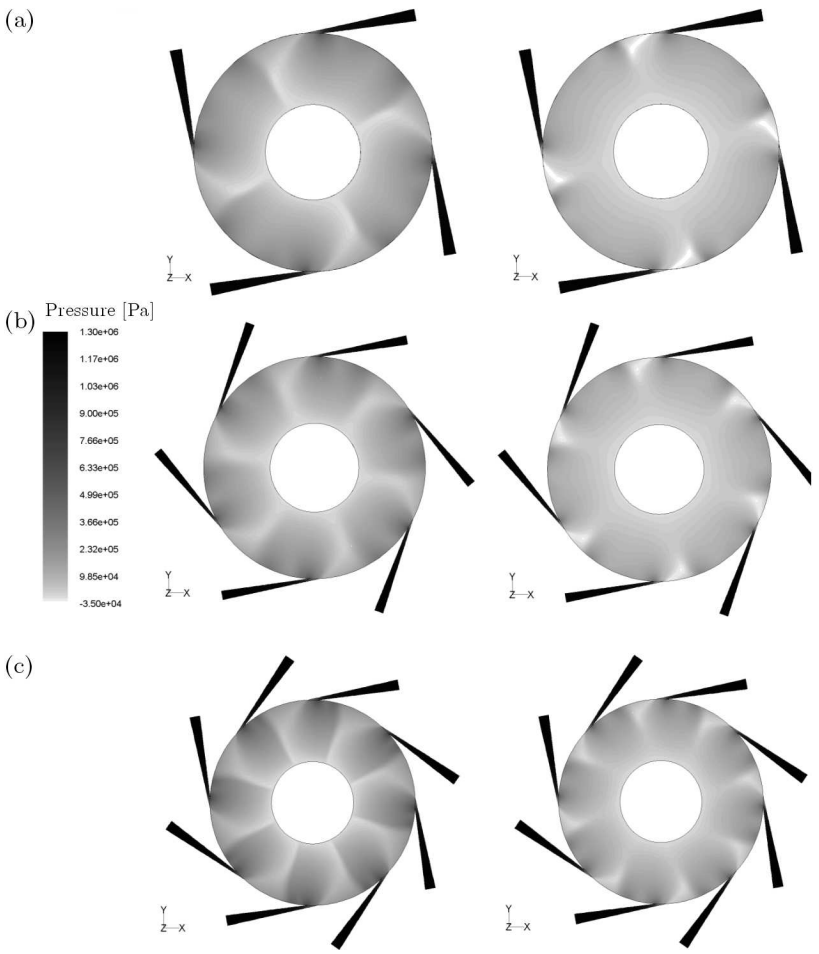

Fig. 5. Contours of static pressure at nominal load, plane of symmetry; four, six and eight nozzle supply, disk diameter 100 mm, inlet angle 10°; (a) 18 000 rpm, (b) 9 000 rpm

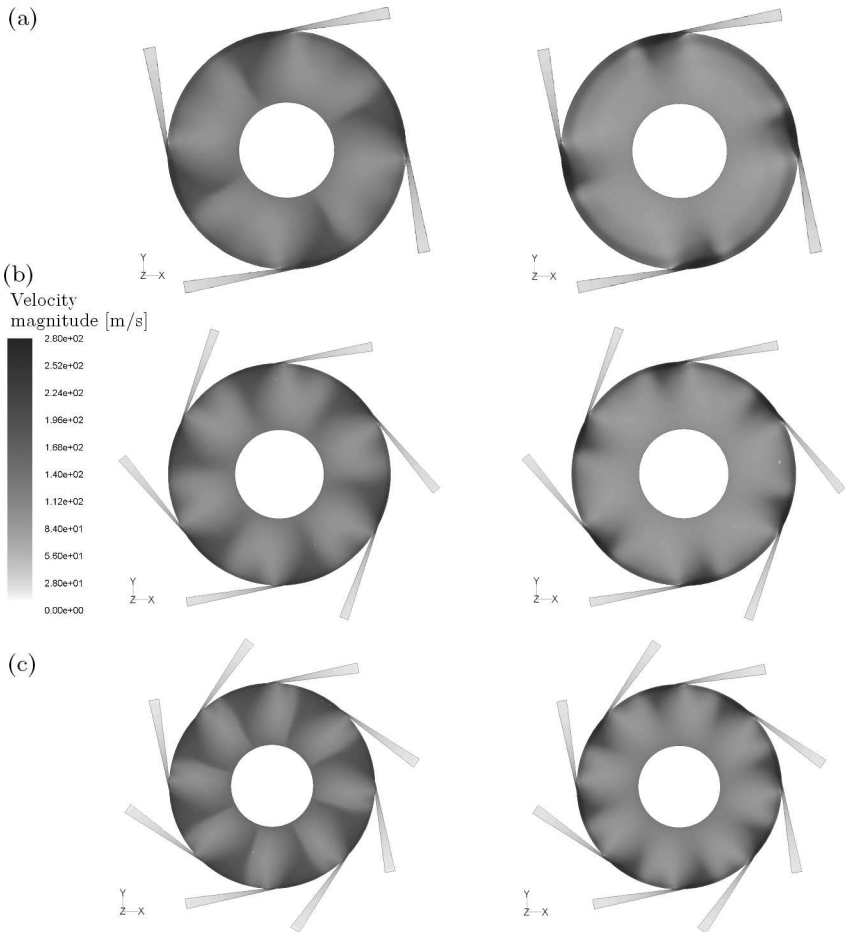

Fig. 6. Contours of velocity magnitude at nominal load, plane of symmetry; four, six or eight supply nozzles, disk diameter 100 mm, inlet angle 10°; (a) 18 000 rpm, (b) 9 000 rpm

pressure drop from 14.9 bar to 1.89 bar). It results from the pressure contours that a part of the available pressure drop is accomplished in the nozzle, the other part takes place in the interdisk space, i.e. in the rotor. Larger pressure drops within the nozzles occur at the rotational speed equal to 9 000 rpm. For this case, further expansion within the rotor leads to a pressure drop just behind the nozzles below the exit value (0.35 bar below the operating conditions of 1.89 bar). For the rotational speed of 18 000 rpm, the lowest value of static pressure is localized at the outlet and the pressure is never lower than the operating pressure. Larger pressure drops along the nozzles for the case of

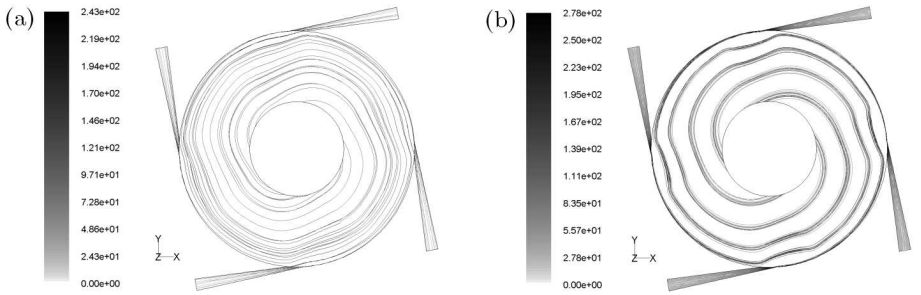

Fig. 7. Pathlines distinguished by the velocity magnitude at nominal load, disk diameter 100 mm, inlet angle 10°; (a) 18 000 rpm, (b) 9 000 rpm

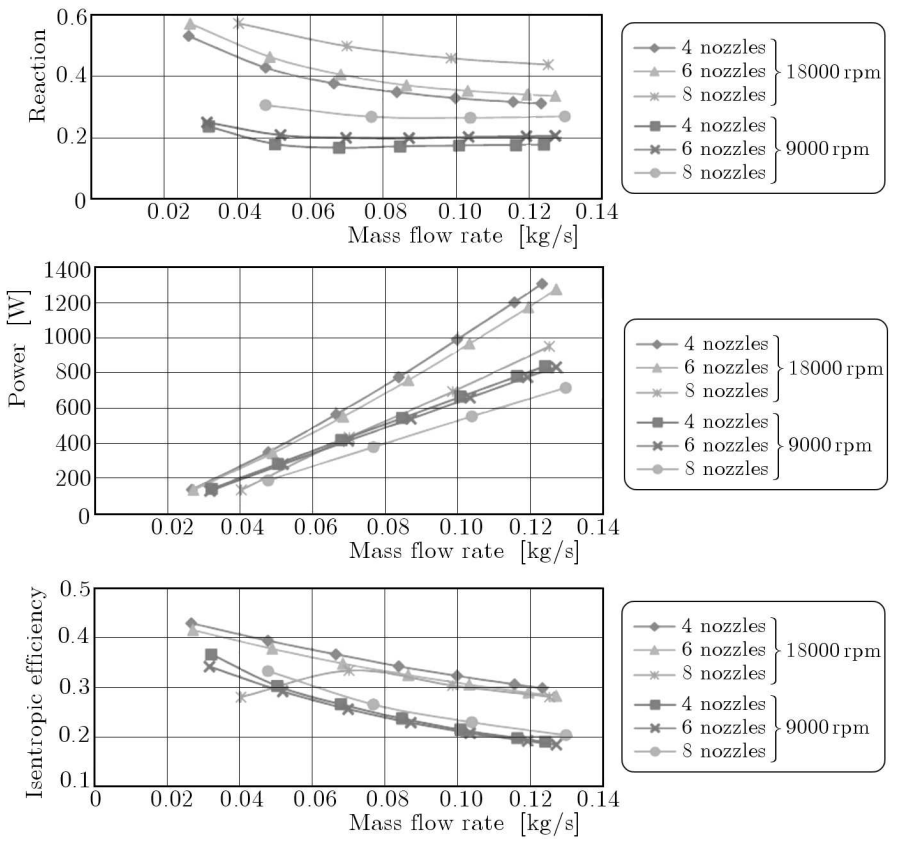

Fig. 8. Degree of reaction, output power and isentropic efficiency of the 11-disk turbine as a function of the flow rate. Diagrams for four, six and eight supply nozzles, disk diameter 100 mm, inlet angle 10°

rotational speed of 9 000 rpm translates onto higher velocities of the working medium at the outlet from the nozzles and at the inlet to the rotor. It reaches 280 m/s then, whereas at the rotational speed of 18, 000 rpm it does not exceed 240 m/s (at the nominal load condition for the Tesla model with four supply nozzles).

Some distance downstream of the nozzles, high gradients of pressure and velocity occur and the configurations of isolines characteristic for the occurrence of shock waves are observed. When a shock wave occurs, an increase of pressure and a decrease of flow velocity takes place. The compression within the shock wave is not desirable in classical bladed turbines. It is a source of losses in the flow.

Streamline patterns for the four-nozzle model (of disk diameter 100 mm) and two rotational speeds of the rotor for the nominal load conditions are presented in Fig. 7. The streamlines are distinguished by the velocity magnitude. Fluid elements move along spiral pathlines from the outer radius to the outlet at the inner radius of the disk. The shape of the pathlines changes with operating conditions (pressure drop in the turbine), rotational speed and the number of supply nozzles. Sample pathlines presented for the case of four nozzle supply are slightly deformed. They are flattened around the nozzle-outlet (rotor-inlet) region due to the influence of flow streams coming out from the nozzles. Fluid elements make up to a few rotations within the interdisk space before they reach the outlet section. For the higher rotational speed of 18 000 rpm where the flow velocity magnitude is lower, it is shown that the spiral pathlines are longer and fluid elements can do 2 revolutions in the space between the rotating disks. 1.25 revolutions are performed for the case of 9 000 rpm. This is consistent with the theory and results of experiments presented in the literature (Praast, 1993). When the turbine is spinning faster, the flow path is longer (and the time of presence of fluid elements in the interdisk region is longer) than in the case when the disks are rotating with a lower velocity. The centrifugal forces increase then. Consequently, the fluid is forced to travel by longer paths and the transfer of energy can be done with a higher efficiency. Finally, the knowledge of the shape of pathlines within the interdisk space can be helpful in better designing of the Tesla turbine disks.

Another conclusion is that in order to reach a high efficiency, the Tesla turbine must have a considerable degree of reaction.

The results of the analysed cases are presented in Fig. 8 as work characteristics, showing main parameters of work like the degree of reaction, output power and isentropic efficiency as a function of mass flow rate. The diagrams concern the models with the disk diameter of 100 mm and inlet angle 10°,

rotating with two rotational velocities. The nominal load conditions are for the pressure drop from 14.8 bar to 1.89 bar and flow rate of 0.13 kg/s. The characteristics show much better conditions (higher flow efficiencies and output power) for the case of 18 000 rpm. The diagram of the degree of reaction shows its increase with the increasing rotational velocity and number of supply nozzles. There is a much lower degree of reaction for the case of 9 000 rpm due to a higher pressure drop in the nozzle region then.

The flow patterns observed within the interdisk space as well as the distribution of reaction are decisive for the obtained output power and isentropic efficiency of the investigated Tesla turbine models. The calculated output power tends to increase with the increasing rotational velocity, however the maximum values of the output power are achieved for the configuration with 4 nozzles, then decreasing with the increasing number of supply nozzles. For 18 000 rpm the output power of the 11-disk turbine reaches 1306 W for the nominal load, while the model working with 9 000 rpm gives only 837 W, which is about 35% lower (the case of 4 nozzle supply, inlet angle 10°, disk diameter 100 mm). The obtained output power depends on the flow efficiency that is reached in the models.

For the rotational speed of 18 000 rpm, the isentropic efficiency along the entire pressure drop characteristic decreases from 43% to 30% at the nominal load, whereas for 9 000 rpm decreases from 37% to 19% only at the nominal load (the case of 4 nozzle supply).

Besides, the models with the inlet angle of 10°, also models with a 15° inlet angle were analysed. It was found that the increased slope angle of the supply nozzles causes a small decrease in the efficiency and output power of the Tesla turbine model. Depending on the number of supply nozzles and rotational speed, the modification of the inlet angle from 10° to 15° causes a 6% to 8% drop of the output power and isentropic efficiency. These values are given for the nominal load and mass flow rate about 0.13 kg/s. The degree of reaction exhibits another trend. In all analysed cases, it is higher in the models with the inlet angle 15° by 3% to 6%, all calculated for the nominal load.

For the investigated models of disk diameter 100 mm, the output power and isentropic efficiency are the highest for the case of 4-nozzle supply. This was also a conclusion of investigations carried out for paper (Lampart *et al.*, 2009) where Tesla models supplied from 1, 2 and 4 nozzles were considered. Thus, vapour supply from 4 nozzles seems to be a very effective way of the Tesla turbine supply.

The numerical results that are presented below are concerned with models of a large disk diameter equal to 300 mm. Models supplied from 2, 4 and 6 nozzles were considered. The analysis was done for the same operating conditions as before, for the same working medium and the same pressure drop from 14.8 bar to 1.89 bar at the nominal point of work. For this large disk diameter, only the rotational speed of 9 000 rpm was considered. Figures 9 and 10 show sample contours of static pressure and velocity magnitude obtained for

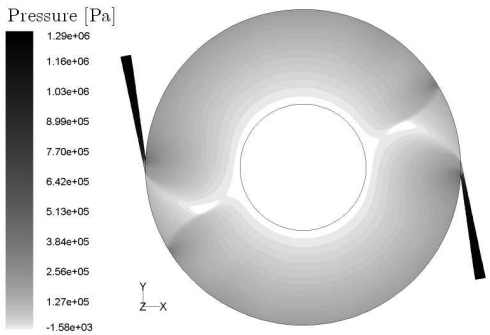

Fig. 9. Contours of static pressure; 2 supply nozzles, disk diameter 300 mm, inlet angle 10°; rotational speed 9 000 rpm

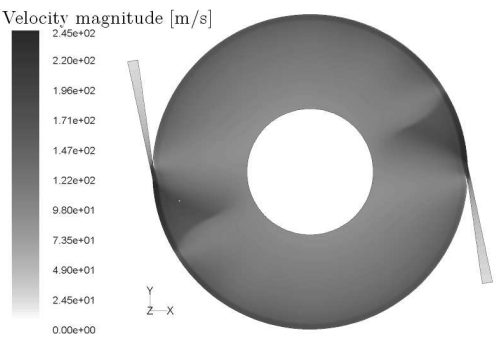

Fig. 10. Contours of velocity magnitude; 2 supply nozzles, disk diameter 300 mm, inlet angle 10°; rotational speed 9 000 rpm

a model supplied from two nozzles. The pictures were captured at the symmetry plane of the interdisk space for the maximum value of flow rate and pressure drop (nominal operating conditions). More less 50% of the available pressure drop is accomplished in the nozzles. The remaining pressure drop takes place between the rotating disks. The enclosed contours of static pressure and velocity exhibit characteristic features that were observed for the smaller

models. There is a zone of large pressure drop and expansion just downstream of the nozzles followed by the shock wave region. Within the shock wave, fluid elements slow down. Downstream they accelerate again under further pressure decrease conditions, then slow down again due to friction effects. After a half revolution, fluid particles are entrained by the inlet stream and are again subject to shock wave conditions occurring downstream of the next nozzle. This cycle will repeat several times along the whole spiral path until the fluid elements reach the outlet, which can also be observed from Fig. 11 showing the shape of pathlines for a 2-nozzle model of diameter 300 mm. As compared to the situation observed for the models with a 100 mm diameter where fluid elements were able to make from 1.25 revolutions for 9 000 rpm to about 2 revolutions for 18 000 rpm before they have reached the outlet, in the model with a diameter of 300 mm the fluid elements perform more revolutions along their pathlines. The number of revolutions for the presented 2-nozzle model is between 5 and 6. As a consequence of the above, the time of passage of fluid elements within the interdisk space is longer than for the smaller models and the kinetic energy of flow can be transferred to the disks with a higher efficiency.

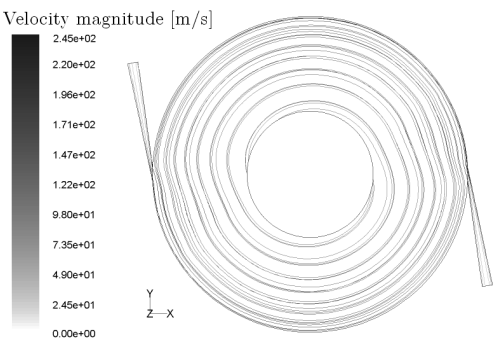

Fig. 11. Pathlines coloured by velocity magnitude; 2 supply nozzles, disk diameter 300 mm, inlet angle 10°; rotational speed 9 000 rpm

Short work characteristics in the form of diagrams of reaction, output power and isentropic efficiency as a function of the mass flow rate for the models with the disk diameter of 300 mm are presented in Fig. 12. The degree of reaction exhibits a similar trend to that observed for the smaller models, however the range of change seems to be wider. The reaction decreases with the increasing mass flow rate. Its maximum value is equal to 0.9 and occurs for the lowest investigated pressure drop. It decreases to 0.24 (two nozzles), 0.26 (four nozzles) and 0.27 (six nozzles), all for the nominal load. The values

of output power are much higher than for the investigated smaller models at the same level of the mass flow rate. For the nominal load, the output power reaches 2235 W for the case of two nozzle supply, 2140 W for four nozzles and 2080 W for six nozzles model. For the investigated models, the increase in the number of supply nozzles gives rise to a small increase of the degree of reaction and a small decrease of the output power for higher values of the flow rate, including the nominal conditions of 0.13 kg/s.

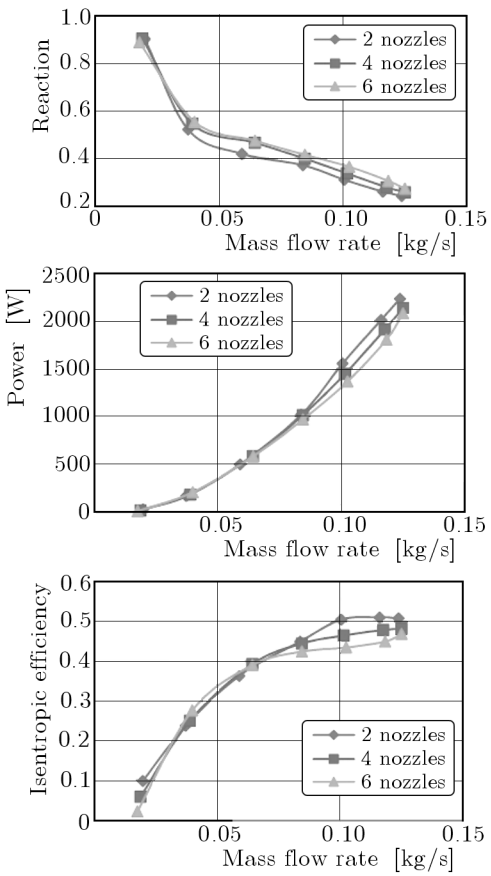

Fig. 12. Work characteristics for the model with a disk diameter 300 mm as a function of flow rate; the system supplied from two, four and six nozzles

The trends observed in the efficiency diagram for large Tesla turbine models (two, four and six nozzle configurations) are different than those found for previously analysed models of disk diameter 100 mm. Here, the isentropic efficiency tends to increase with the increasing value of the mass flow rate and "saturate" near the nominal operating conditions. The maximum obtained va-

lues of efficiency are much higher than for the smaller models. The isentropic efficiency for the nominal turbine load is equal to 51% for the 2-nozzle model, 48% for the 4-nozzle model and 47% for the 6-nozzle model. This is to confirm our earlier predictions that the increased number of revolutions that fluid elements perform within the interdisk space and longer pathlines of fluid elements in large diameter models enable more efficient transfer of power from the flow to the disk. All the received values of efficiency for different models of disk diameter 100 mm and 300 mm are gathered in Table 2.

Table 2. Efficiency comparison for all calculated models (at nominal load)

Nozzle configuration	Diameter of the disk	18 000 rpm	9 000 rpm
4 nozzles, 10°	100 mm	30%	19%
4 nozzles, 15°	100 mm	28%	18%
6 nozzles, 10°	100 mm	28%	18%
6 nozzles, 15°	100 mm	26%	17%
8 nozzles, 10°	100 mm	24%	16%
8 nozzles, 15°	100 mm	23%	16%
2 nozzles, 10°	300 mm	–	51%
4 nozzles, 10°	300 mm	–	48%
6 nozzles, 10°	300 mm	–	47%

5. Full model analysis

Besides the simplified models of Tesla turbines, also a full model of an 11-disk turbine working on a low boiling medium SES36 was prepared. A half of the real 11-disk turbine was calculated under the assumption of symmetry of the construction. The disks are located in the casing. There are radial gaps above the disks. The outlet from the turbine is accomplished through four holes situated in each disk (save for the central disk) near the shaft. These holes allow the outflow of the medium in the axial direction. Let us recall that in the simplified model, the working fluid was assumed to outflow directly to the shaft. Under the symmetry conditions, the medium leaves the turbine to the left and right, so there are no axial forces acting on the shaft and bearings. The turbine model is supplied from four nozzles and the inlet angle is assumed equal to 10°, as in the investigations of the simplified models. The interdisk

space is still the same, 0.25 mm. The fact that the clearances above the disks are not ignored is a considerable modelling improvement over the simplified models, allowing the leakage over the disks to be taken into account. The whole model contains above 7.5 million finite volumes.

The same set of pressure drops up to the highest drop (from 14.8 bar to 1.89 bar) was used as a boundary condition. The image presented in Fig. 13 shows the static pressure in the symmetry plane in one interdisk space for the

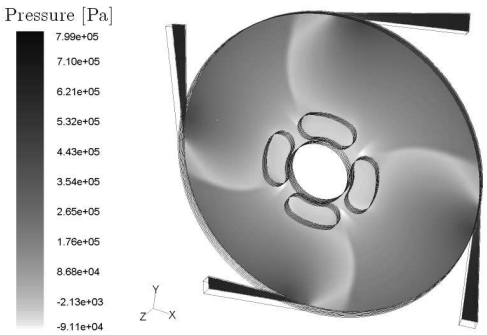

Fig. 13. Full model calculations. Contours of static pressure in the symmetry plane between the disks

inlet pressure of 8 bar. The expansion along the nozzles is weaker than in the case of the simplified model investigated earlier. The pressure drop realised in the interdisk spaces is larger which suggests a higher value of reaction. The distribution of static pressure between the disks presented in Fig. 14 shows an

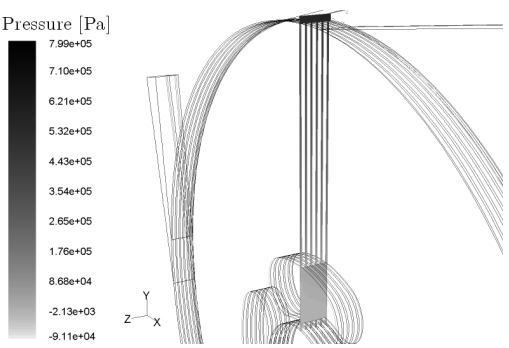

Fig. 14. Full model calculations. Change of static pressure in the neighbouring disks

asymmetric character. The pressure between the disks inside the turbine, close to the central disk (without holes) is higher than that between the side disks, near the casing. Subsequent disks are not uniformly loaded. The investigated

model assumes the same area of the outlet holes in each disk. Thus, the outlet holes in side disks exhibit higher values of mass flow rate, coming also from the preceding interdisk domains. Arranging the individual size of the outlet holes in each disk can lead to a more uniform loading of the disks.

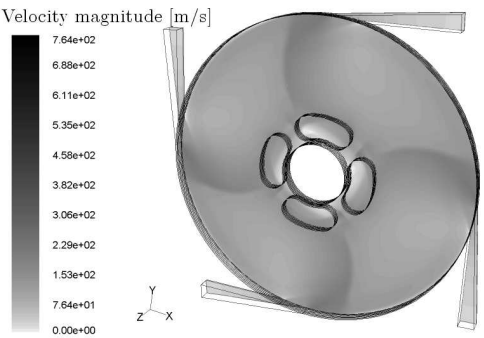

Fig. 15. Full model calculations. Distribution of the velocity magnitude in the symmetry plane between the disks

Static pressure contours in Fig. 13 and also velocity contours presented in Fig. 15 show the occurrence of shock waves within the interdisk space. Similar to the situation observed for the simplified models, the fluid elements pass through shock wave zones several times along their pathlines within the interdisk space.

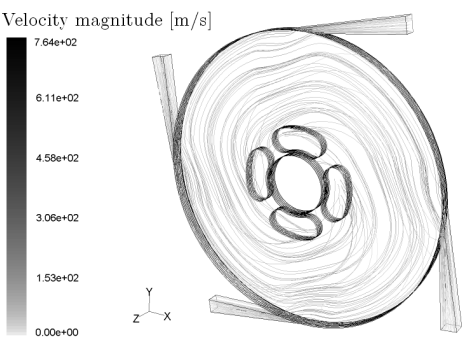

Fig. 16. Full model calculations. Pathlines distinguished by the velocity magnitude in the symmetry plane between the disks

The analysis of pathlines presented in Fig. 16 shows some similarities to the simple models. The working medium flows along spiral pathlines from the nozzle outlets (at the outer radius) to the outlet holes (near the inner radius). The number of revolutions done by fluid elements is smaller than in the corresponding simplified models, with the disk diameter of 100 mm. For

18 000 rpm it is not more than 1.5 revolutions before reaching the outlet holes, whereas in the simplified models, with the disk diameter of 10 cm, it was 1.25 for 9 000 rpm and around 2 for 18 000 rpm. The number of revolutions done by the fluid elements in the intedisk space strongly affects the flow efficiency of the Tesla turbine. The highest isentropic efficiency values were found in situations where the time of presence of the working fluid between the disks was the longest. As a consequences, the flow efficiency of the full model geometry is relatively low. It amounts to 16% only at the nominal point of work (mass flow rate of 0.13 kg/s), which is almost by half less than the value of isentropic efficiency obtained for the simplified model (found there as 30% for the case of 4 nozzle supply).

Figures 13-16 also exhibit the presence of strong swirls in the zone of outlet holes which add to a low efficiency of the model. In this region, the direction of flow changes rapidly from spiral in the radial plane to axial. The outlet holes are spinning together with the disks and this is another reason for formation of eddies at the outlet from the Tesla turbine. It is also important to note that the zone of the lowest pressure is located not in the outlet holes but between the outlet holes. The presented full model geometry is in an early stage of development and several improvements must be implemented. First of all, the diameter of the outlet holes must vary with disk location in the turbine to obtain the same pressure drop and value of flow rate in all interdisk spaces. Also the location of the supply nozzles at the disk circumference should be synchronised well with the location of the outlet holes. This is not an easy task, however tracing the shape of the fluid elements pathlines in the interdisk space may be helpful. Also to better understand all the flow phenomena taking place in the Tesla turbine, full unsteady calculations must be performed.

6. Summary

Results of analysis presented in this paper show a unique character of operation of the Tesla bladeless turbine. Different types of models divided into two main groups were analysed, including a group of simplified models and a group of full geometry models. Within the first group of models, only a half of a single interdisk space was transformed into the calculation domain, assuming the symmetry of flow between the disks, and assuming an infinite number of disks. The outlet from the interdisk space was realised directly to the shaft. Turbine models differed in disk diameter (100 and 300 mm), rotational speed (9 000 and 18 000 rpm) and nozzle configuration. The models were supplied

from four, six and eight nozzles located along the circumference for two inlet angles (10° and 15°). Models of the second group were prepared without the simplifications assumed for the first group of models. The outlet from interdisk channels was performed through the several outlet holes in disks located near the shaft. The radial gap above the disks was also taken into consideration. In this group, the inlet angle of 10° and the disk diameter of 100 mm was assumed.

All the analysed models were assumed to operate on a low boiling medium, SolkathermSES36 in an organic Clausius-Rankine cycle. The nominal point of work was designed at 0.13 kg/s of the mass flow rate of the working fluid (overheated steam of low boiling medium) and pressure drop from 14.8 bar to 1.89 bar. The number of co-rotating disks was assumed as 11.

The calculations exhibit interesting features of transonic flow in the high-load Tesla turbine. Fluid elements pass through shock wave zones several times along their pathlines within the interdisk space.

For simple models with a small diameter of the disks (100 mm), the highest value of isentropic efficiency was achieved in the model supplied from four nozzles for the inlet angle of 10° and rotational velocity of 18 000 rpm. It reached 30% for the nominal load, giving 1 300 W of the output power. It was found that a further increase of the number of nozzles has an adverse impact on flow efficiency. Since in the previous analysis of one, two and four nozzle models the maximum efficiency was also found for the four nozzle arrangement (Lampart *et al.*, 2009), the four-nozzle supply system seems to be the optimum configuration for the investigated model. A change of the inlet angle from 10° to 15° gives a small efficiency decrease for the model turbine. The rotational speed of the disks also seems to be a very important factor, if talking about the output power and flow efficiency. It has an influence on the shape of streamlines and the total time of presence of fluid elements between the disks. A higher efficiency was observed at the higher rotational speed of 18 000 rpm, where the pathlines were by about 50% longer than those in the case of 9 000 rpm.

The efficiency value of 30% obtained for the investigated 100 mm model is still not satisfying for the Tesla turbine to be competitive as compared with classical bladed turbines. In order to improve the flow efficiency, models with the disk diameter of 300 mm were also investigated, showing some improvements in the shape of streamlines and flow efficiency. The best results were obtained for the model with two nozzles, 10° inlet angle and 9 000 rpm. The calculated flow efficiency reached over 50% at the nominal load (for the same mass flow rate as for 100 mm models) as fluid elements perform up to 6 revolutions before reaching the outlet.

The numerical analysis of the full 100 mm model yields at the moment the isentropic efficiency of 16% only at the nominal load, which is much smaller than for the simplified model. This is because in the tested models, there is a non-uniform loading of the subsequent disks. Pathlines of the fluid elements within the interdisk spaces are relatively short and there are strong eddies in the outlet holes zone. Several improvements, including variation of the area of outlet holes from disk to disk and synchronisation of the supply nozzles with the location of the outlet holes are needed to considerably improve the flow efficiency of the models.

Acknowledgements

The calculations of the full Tesla turbine model presented in this paper have been done on the Galera supercomputer of the TASK Centre.

References

1. Beans W.E., 1966, Investigation into the performance characteristics of a friction turbine, *Journal of Spacecraft and Rockets*, **3**, 1, 131-134
2. Davydov A.B., Sherstyuk A.N., 1980, Experimental research on a disc microturbine, *Russian Engineering Journal*, **8**
3. Fluent Inc., 2000, *Fluent/UNS/Rampant, "User's Guide"*
4. Fluent Inc., 2000, *Gambit. "User's Guide"*
5. Gruber E.L., 1960, *An Investigation of a Turbine with a Multiple Disc Rotor*, Thesis, Arizona State University, Tempe, Arizona
6. Hicks K., 2005, *Method of and apparatus for a multi-stage boundary layer engine and process cell*, United States Patent US 6,973,792 B2, Dec. 13
7. Kosowski K., 2007, *Steam and Gas Turbines with Examples of Alstom Technology*, 2nd edition, Alstom Power Sp. z o.o.
8. Lampart P., Kosowski K., Piwowarski M., Jędrzejewski Ł., 2009, Design analysis of a Tesla micro-turbine operating on a low-boiling medium, *Polish Maritime Research*, Sp. Issue No. 1, 28-33
9. Menter F.R., Kuntz M., Langtry R., 2003, Ten years of industrial experience with the SST turbulence model, *Turbulence, Heat and Mass Transfer*, **4**, Begell House, Inc.
10. Mikielewicz J., Kosowski K., Lampart P., Piwowarski M., Bykuć S., 2008, *Analiza możliwości zastosowania turbiny Tesli w mikrosiłowni z czynnikiem niskowrzącym*, The Szewalski Institute of Fluid-Flow Machinery, Gdańsk

11. NORTH R.C., 1969, *An Investigation of the Tesla Turbine*, Thesis, University of Maryland

12. PRAAST T.D., 1993, Theory and plans for the Tesla turbine, *TMMI 1315 Pepper Drive*, **7**, El Cajon CA 92021-1425

13. RICE W., 1965, An analytical and experimental investigation of multiple-disk turbines, *Journal of Engineering for Power, Trans. ASME*, 29-36

14. RICE W., 1991, Tesla turbomachinery, *Conference Proceedings of the 4th International Tesla Symposium*, Serbian Academy of Sciences and Arts, Belgrade, Yugoslavia, 117-125

15. TESLA N., 1913, *Turbine*, Patent no: 1,061,206., United States Patent Office, of New York N. Y., Patented May 6

16. WILCOX D.C., 1993, *Turbulence Modelling for CFD*, 2ed., DCW Industries, Inc., La Canada, CA

Badania aerodynamiki bezłopatkowych mikroturbin typu Tesli

Streszczenie

W pracy przedstawiono analizę bezłopatkowej turbiny tarczowej Tesli pracującej w organicznym obiegu Rankine'a z czynnikiem niskowrzącym w mikrosiłowni kogeneracyjnej o mocy cieplnej 20 kW. Wykonano obliczenia numeryczne przepływu w turbinie Tesli w szerokim zakresie zmienności parametrów pracy turbiny. Wyniki badań obrazują szereg ciekawych cech w rozkładzie parametrów przepływu w przestrzeniach międzytarczowych turbiny. Sprawność turbiny Tesli zależy od wielu parametrów przepływowych, takich jak ciśnienie, temperatura, prędkość czynnika, prędkość obrotowa wirnika, oraz od wielu parametrów geometrycznych, m.in. od liczby i średnicy tarcz, odległości między tarczami, stanu powierzchni tarcz oraz układu dysz zasilających. Obliczone sprawności modeli turbiny Tesli wskazują, że najlepsze rozwiązania tej turbiny mogą konkurować z klasycznymi turbinami łopatkowymi.

Manuscript received September 13, 2010; accepted for print November 25, 2010